Title

Rapid acting antidepressant (2R,6R)-hydroxynorketamine (HNK) targets glucocorticoid receptor signaling: a longitudinal cerebrospinal fluid proteome study

Authors

David P. Herzog[1,*] MD; Natarajan Perumal[2,*] PhD; Caroline Manicam[2] PhD; Giulia Treccani[1,3,4] PhD; Jens Nadig[1]; Milena Rossmanith[2]; Jan Engelmann[1] MD; Tanja Jene[1] MS; Annika Hasch[1] MS; Michael A. van der Kooij[1,5] PhD; Klaus Lieb[1,5] MD; Nils C. Gassen[6] PhD; Franz H. Grus[2] MD PhD; Marianne B. Müller[1,5] MD

Affiliations

[1]Department of Psychiatry and Psychotherapy and Focus Program Translational Neurosciences, Johannes Gutenberg University Medical Center Mainz, Mainz, Germany.

[2]Experimental and Translational Ophthalmology, Department of Ophthalmology, Johannes Gutenberg University Medical Center, Mainz, Germany.

[3]Institute for Microscopic Anatomy and Neurobiology, Johannes Gutenberg University Medical Center, Mainz, Germany.

[4]Translational Neuropsychiatry Unit, Department of Clinical Medicine, Aarhus University, Risskov, Denmark.

[5]Leibniz Institute for Resilience Research, Mainz, Germany.

[6]Neurohomeostasis Research Group, Department of Psychiatry and Psychotherapy, University Medical Center Bonn, Bonn, Germany.

*Shared first authorship in alphabetical order.

Corresponding author

David P. Herzog, MD

Laboratory of Translational Psychiatry

Department of Psychiatry and Psychotherapy

Johannes Gutenberg University Medical Center Mainz

Hanns-Dieter-Hüsch-Weg 19

55128 Mainz, Germany

Phone: +49 6131 39 21345

Fax: +49 6131 39 29815

Email: daherzog@uni-mainz.de

Conflict of interest statement

The authors have declared that no conflict of interest exists.

Abstract

Delayed onset of antidepressant action is a shortcoming in depression treatment. Ketamine and its metabolite (2R,6R)-hydroxynorketamine (HNK) have emerged as promising rapid-acting antidepressants. However, their mechanism of action remains unknown. In this study, we first described the anxious and depression-prone inbred mouse strain, DBA/2J, as a animal model to assess the antidepressant-like effects of ketamine and HNK *in vivo*. To decode the molecular mechanisms mediating HNK's rapid antidepressant effects, a longitudinal cerebrospinal fluid (CSF) proteome profiling of its acute and sustained effects was conducted using an unbiased, hypothesis-free mass spectrometry-based proteomics approach. A total of 387 proteins were identified, with a major implication of significantly differentially expressed proteins in the glucocorticoid receptor (GR) signaling pathway, providing evidence for a link between HNK and regulation of the stress hormone system. Mechanistically, we identified HNK to repress GR-mediated transcription and reduce hormonal sensitivity of GR *in vitro.* In addition, mammalian target of rapamycin (mTOR) and brain-derived neurotrophic factor (BDNF) were predicted to be important upstream regulators of HNK treatment. Our results contribute to precise understanding of the temporal dynamics and molecular targets underlying HNK's rapid antidepressant-like effects, which can be used as a benchmark for improved treatment strategies for depression in future.

Introduction

A well-recognized shortcoming of currently available pharmacological agents in the treatment of major depressive disorder (MDD) is that significant difference from placebo can only be reliably identified 4-6 weeks after treatment onset (1). This therapeutic delay of classical antidepressants is potentially dangerous since suicide risk is the highest in the early treatment period when the disease severity is at its greatest (2). The absence of rapid positive feedback also encourages non-compliance, thus increasing duration of the depressive episode and the overall costs for treating this disease (3). In addition, the lack of biomarkers for disease monitoring or drug choice in the clinical setting is a major drawback in depression treatment (4).

In search for putative targets mediating a more rapid antidepressant response, *N*-methyl-D-aspartate (NMDA) receptor antagonists, with ketamine as a prototypical agent, have gained increasing interest during the last years (5). Sub-anesthetic doses of the narcotic agent ketamine have been shown to produce both rapid (within hours) and sustained (up to 1 week) antidepressant effects in patients (6) and rodents (7). In addition, there is convincing evidence from clinical trials that ketamine is also effective in patients with treatment-resistant depression (8). Besides its activity at the NMDA receptor, several putative molecular mechanisms through which the antidepressant-like effects of ketamine are mediated have been discovered, including the involvement of mechanistic target of rapamycin complex 1 (mTORC1) signaling and acute modulation of brain-derived neurotrophic factor (BDNF) release (9).

Despite its proven antidepressant efficacy even in difficult-to-treat patients, a broad range of side effects, including strong sedation, dissociation, nausea, and the risk of addiction have prevented ketamine to be widely used so far (10). Recent preclinical studies indicate that the

ketamine metabolite, (2*R*,6*R*)-hydroxynorketamine (HNK), retains the rapid and sustained antidepressant-like effects in rodents, but lacks its dissociative-like properties and abuse potential (11-13). Therefore, HNK is a potential prototypical candidate to be further tested and developed as a rapid-acting antidepressant agent. However, for HNK, which does not block NMDA receptors like ketamine (14), the molecular signaling mechanisms still remain largely unknown (15). In addition, the antidepressant-like effects of HNK could not always be reproduced by research groups around the world. We summarized the evidence in a recent review (16). To date, systematic studies aiming at the hypothesis-free identification of proteins and signaling pathways involved in HNK's rapid onset of action are yet to be reported.

Despite considerable efforts, biomarker candidates to support clinical diagnosis or treatment response that could finally support decision-making within MDD diagnosis and therapy guidelines are still lacking (17). Access to the organ of interest as source for biomaterial, i.e. the brain, is restricted, if not impossible. Data on peripheral blood-based biomarkers and molecular candidates have been relatively inconclusive so far, and peripheral changes are remarkably different from the molecular changes that are observed within the central nervous system (e.g. (18)). Cerebrospinal fluid (CSF) is an accessible biological fluid in both humans and rodents that is circulating in close vicinity to the brain. In the past decade, technological advancement and the increasing quality of unbiased "omics" approaches have facilitated the use of CSF for biomarker research and investigations into disease-related pathophysiological processes. However, in contrast to other mental diseases such as neurodegenerative disorders where CSF is traditionally an established source for biomarker research, only very few investigations have used CSF to monitor the changes in the context of antidepressant treatment.

In 2014, Onaivi *et al.* described an animal experimental approach using intraventricular cannulation to enable serial CSF withdrawal in conscious mice (19). The suitability of this approach was validated by revealing specific proteomic signatures in murine CSF samples following acute stress and acute cocaine administration (19). In the current study, we adopted this method to focus on temporal changes of the CSF proteome induced by systemic administration of an antidepressant-like dosage of HNK. As animal model system, we chose male DBA/2J mice. This inbred mouse strain is characterized by high innate anxiety, which can be successfully treated by commonly used antidepressants (18, 20, 21). Moreover, the DBA/2J mice display a reduced inhibitory HPA axis feedback (22) closely mimicking this impairment in depressed humans. Choosing an antidepressant-responsive strain enables experiments to be performed under baseline conditions i.e. without the need to apply additional and potentially confounding stressors to shift the behavioral phenotype of the animals to a depressive-like state to model disease-like conditions (18). Here, we performed serial CSF sample collection from conscious and freely moving mice in a longitudinal study design to identify the proteome changes closely associated with changes in brains states following administration of HNK over time. Changes in the CSF proteome and differential expression of proteins associated with the acute (4 hours after injection) and sustained (1 week after injection) antidepressant-like effects of a single injection of HNK or saline were further investigated employing a hypothesis-free, unbiased mass spectrometry-based proteomics approach.

Results

Behavioral profiling of ketamine and HNK in DBA/2J mice

With this behavioral experiment, we wanted to first validate that DBA/2J inbred mice are a suitable strain and model organism to investigate the antidepressant-like effects of ketamine and HNK. DBA/2J mice displayed a depression-like phenotype under control conditions with high immobility scores in the FST (Figure 1A and B at 4h and 1w, respectively; saline-treated animals). At both *acute* and *sustained* time points, ketamine and HNK induced significant antidepressant-like effects by reducing immobility time (Figure 1A and B). We detected no statistically significant differences between the effects of HNK and ketamine at both time points (Figure 1A and B).

Locomotor activity is known to be impaired by ketamine treatment and constitutes an important side-effect of ketamine (10). Indeed, ketamine-induced reduction in general locomotor activity could be visualized by an altered tracking profile in the OF test during 30 minutes of post-injection recording (Figure 1C). Furthermore, ketamine reduced the total distance travelled, compared to HNK and saline injection (Figure 1D).

Acute and sustained effects of HNK on CSF proteome

CSF is in close vicinity to the brain, and there is a continuous exchange and molecular crosstalk between brain tissue and CSF. Because of the clear behavioral effects of HNK and the fact that so far, data about its mechanism of action remain fragmentary, we decided to exclusively focus on HNK and analyze the CSF samples obtained from conscious DBA/2J mice treated with HNK or saline. As part of the method validation, we investigated whether the CSF withdrawal procedure was stressful for the animal by measurement of plasma CORT

concentrations in an independent experiment. The mean peak level of CORT from mice which underwent the CSF withdrawal procedure was 84.84 ng/ml (Figure S1), not exceeding average plasma CORT concentrations reached following exposure to a novel environment, such as a commonly used OF test (23).

In the main experiment, CSF samples were pooled (Supplemental data A), processed, and subjected to first dimensional gel electrophoresis (1DE), as depicted in Figure S2. In total, 387 proteins were identified from both *Mus musculus* (309 proteins) and *Homo sapiens* (229 proteins) databases by label-free quantification at a false discovery rate (FDR) of 1% (Figure 2A; full data in Supplemental data C-E). As many as 151 proteins were found to be overlapping in both databases, as shown in the Venn diagram (Figure 2A). The use of both mouse and human UniProt databases maximized protein identification due to limited annotations in the mouse database (17 001 proteins) compared to the human database (20 410 proteins).

Among these murine CSF proteins, 25 and 65 proteins were found to be differentially expressed at 4 hours (Figure 2B) and 1 week (Figure 2C) after HNK treatment compared to saline (for comprehensive list see Supplemental data F and Figure S3). Nine proteins were upregulated following 4 hours HNK administration namely cytoskeletal structural protein dynein light chain 2, cytoplasmatic (Dynll2), proteasome subunit beta type 2 (Psmb2), apolipoprotein (Apoe), and spine growth modulator protein transforming protein RhoA (Rhoa). Sixteen proteins were downregulated following 4 hours HNK versus saline injection (Figure 2C), mainly cytoskeletal keratins consisting of keratin type II cytoskeletal 1, 2 peridermal, 2 oral, 9, 10 (KRT1, KRT2, KRT76, KRT9, KRT10), myelin proteins composed of myelin basic protein (Mbp) and myelin proteolipid protein (Plp1), signaling protein 14-3-3 protein sigma (Sfn), and myelinotrophic and neurotrophic factor prosaposin (Psap). One week

following HNK injection, we found 41 proteins to be upregulated (Figure 2C). Examples of these proteins were Mbp, Plp1, glial fibrillary acidic protein (Gfap), amino acid transporters ADP/ATP translocase 2 (SLC25A5) and 1 (Slc25a4), cytoskeletal proteins actin-related protein 2/3 complex subunit 4 (Arpc4), vimentin (Vim), tubulin beta-5 chain (Tubb5), plasma kallikrein (Klkb1), moesin (Msn), and transcription factor putative elongation factor 1-alpha-like 3 (EEF1A1P5). A total of 24 proteins were downregulated comprising mainly cytoskeletal keratins (KRT1, 9, 6A, 10), mitochondrial proteins electron transfer flavoprotein subunit alpha (ETFA), malate dehydrogenase (Mdh2), stress-70 protein (HSPA9), 4-aminobutyrate aminotransferase (Abat), aconitate hydratase (Aco2), pyruvate dehydrogenase E1 component subunit beta (PDHB), Na/K-transporting ATPase subunit alpha-1 (ATP1A1), cholinergic neuron ATP-binding protein in neurons phosphatidylethanolamine-binding protein 1 (Pebp1), and chaperone heat shock protein a5 (HSPA5). Further clustering of these differentially expressed CSF proteins depicted as heat maps with unsupervised hierarchical clustering demonstrated the segregation of identified proteins into two major clusters according to the respective time points (Figure 2D). Three distinct protein expression profiles were observed. First, the expression of a cluster pf proteins remained the same at both 4h and 1w composed of down-regulation of KRT1, KRT9, and KRT10, and the up-regulation of Rbp4. The second cluster consisted of proteins that were upregulated following 1w of HNK administration comprising Mbp and PLP1. The third cluster was characterized by expression of proteins that were only regulated exclusively at either time point. Conducting a protein-protein interaction network (PPI) analysis, we could show the localization in particular cellular compartments and molecular types (Figure S3). Interestingly, the protein group observed to have the highest interaction parterns consisted of keratins (Figure S3).

In an attempt to further explore the functional relevance of the proteins identified to be differentially expressed, canonical pathway enrichment was determined employing the IPA tool using a cut-off of $p<0.05$. The 21 proteins following 4 hours HNK injection were significantly associated with the glucocorticoid receptor (GR) signaling (p = 1.52E-03; Figure 3A). On the other hand, 9 top canonical pathways were found to be differentially regulated by the 57 differentially expressed proteins following 1 week HNK treatment, as shown in Figure 3A. Among these, the acute phase response signaling (p = 5.30E-11) was the most significantly implicated pathway, followed by unfolded protein response (p = 3.07E-04), clathrin-mediated endocytosis signaling (p = 2.17E-03), GR signaling (p = 2.35E-03), 14-3-3 mediated signaling (p = 3.68E-03), glycolysis I (p = 1.21E-02), gluconeogenesis (p = 1.21E-02), and signaling by the Rho family GTPase (p = 2.13E-02). Noteworthy, the GR signaling-associated proteins at both time points comprised mainly a cluster of keratins and heat shock proteins. Among the keratins, KRT1, KRT9, and KRT 10 were consistently downregulated at both time points, whereas KRT76 and KRT2 were exclusively downregulated at 4 hours and KRT6A at 1 week after HNK treatment (Figure 3B; Supplemental data G).

HNK represses GR-mediated transcription and reduces hormonal sensitivity of GR *in vitro*

We were interested how HNK affected GR translational activity and GR response to glucocorticoids in neuronal cells. We performed an *in vitro* gene reporter assay assessing GRE-driven transcriptional activity by transient transfection of MMTV-Luciferase construct into HT-22 mouse hippocampal neuronal cells and found that HNK represses GR-mediated transcription in a glucocorticoid (DEX) dependent manner (Figure S4). We detected no direct effect of HNK on GR-activity, when steroids were withdrawn from culture medium (Figure

S4). Moreover, we found a reduced hormonal sensitivity of GR when cells were co-treated with HNK compared to control condition (Figure 3C).

Figure 4 depicts the further analysis of the top disease and biological functions associated with the differentially expressed CSF proteins at both time points. At 4h after HNK treatment, myelination (p = 2.43E-03; Figure 4B), regeneration of neurons (p = 4.32E-03), and organization of filaments (p = 1.04E-02) were found to be significantly affected. The subacute effect of HNK administration after 1w demonstrated that the proteins found to be differentially expressed were significantly associated with top eight networks involved in Alzheimer disease (p = 1.93E-07; Figure 4C), organization of filaments (p = 6.36E-05; Figure 4D), schizophrenia (p = 2.36E-04), gluconeogenesis (p = 7.17E-04), neurological signs (p = 7.35E-04), proliferation of neuroglia (p = 2.01E-03), Parkinson´s disease (p = 4.03E-03), and regeneration of neurons (p = 1.75E-02). Finally, we analyzed the predicted upstream regulators to identify the molecules, including transcription factors, which were significantly involved in the regulation of the differentially expressed proteins in both groups. Interestingly, at the 4h time point, the major regulators were all inhibited comprising insulin like growth factor 1 (IGF1) (p = 7.7E-05; z-score = -2.18), mTOR (p = 1.2E-05; z-score = -0.475), tumor necrosis factor (TNF) (p = 1.6E-04; z-score = -0.743) and transforming growth factor beta 1 (TGFβ1) (p = 2.5E-02; z-score = -0.152), as depicted in Figure 5A. However, at the 1 w time point following HNK treatment, five upstream regulators were predicted to be activated, which were interleukin 6 (IL6) (p = 1.2E-05; z-score = 1.337), IGF1 (p = 1.7E-04; z-score = 1.28), TNF (p = 3.9E-03; z-score = 0.742), mTOR (p = 1.2E-03; z-score = 0.243), and BDNF (p = 1.2E-04; z-score = 0.128; Figure 5B). Three regulators comprising transforming growth factor alpha (TGFα) (p = 5.0E-05; z-score = -0.257) and TGFβ1 (p =

3.4E-04; z-score = -0.24), and androgen receptor (AR) (p = 2.8E-05; z-score = -0.283) were inhibited. It is noteworthy that mTOR was inhibited at 4 h (Figure 5C) but activated at 1w (Figure 5D). Correspondingly, the expression pattern of myelin protein Plp1, which is a common molecule at both time points, decreased at 4 h but increased at 1 w.

Discussion

The present study provides first evidence that the DBA/2J mouse strain is a suitable animal model to assess the antidepressant-like effects of rapid-acting antidepressants such as ketamine and HNK. In a next step, we successfully used this model to decode the molecular mechanisms underlying HNK's rapid acting properties: we characterized the signature and longitudinal changes in the CSF proteome of conscious mice following systemic injection of HNK, which is the most promising metabolite of ketamine. Mechanistically, we identified GR signaling as a putative novel candidate mechanism through which both acute and sustained antidepressant-like effects of HNK might be mediated, thus revealing an intriguing functional link between HNK's antidepressant mechanism of action and targeted regulation of the stress hormone system.

Acute and sustained antidepressant-like properties of HNK: importance of experimental model system

In 2016, Zanos *et al.* first described the antidepressant-like properties of HNK (13), which was then further investigated and developed as a putative rapid-acting antidepressant compound with a more favorable side-effect profile than ketamine (11, 12). However, while antidepressant-like effects of ketamine in rodents are relatively robust, the behavioral effects of HNK are more inconsistent and seem to depend on different parameters within the experimental conditions and the mouse strain used (24). Most of the recent studies on ketamine and HNK applied experimental depression models, such as stress or chronic inflammation (16). For example, Chou *et al.* used a learned helplessness paradigm to induce a depressive-like phenotype in rats and demonstrated that HNK decreased depression-like

behavior independent of gender (11). Another study using a lipopolysaccharide model of depression was not able to detect any antidepressant-like effects of HNK that were comparable to those of ketamine in male C57/BL6J mice (25). One plausible explanation for those inconsistencies of behavioral effects of HNK in rodents might be the use of different strains and experimental disease models and approaches to mimic clinically relevant conditions.

Adding to this, we could show for the first time, that a single dosage of HNK is equally effective as ketamine in inducing both acute and sustained antidepressant-like effects in DBA/2J mice. Saline-injected animals (i.e. vehicle controls) showed a depression-like behavioral phenotype, which could be attenuated by administration of ketamine and HNK. The clear antidepressant-like effect of both compounds is probably due to the innate high anxiety-like behavior of this inbred mouse strain, which has proven its particular value in psychopharmacological research into antidepressant mechanisms of action (18). Therefore, it is surprising to see that for the rapid-acting compound ketamine and its metabolite HNK, many studies published so far used the C57/BL6 strain, which, under baseline conditions, does not show a typical depression-like behavioral phenotype. Our data support that the DBA/2J strain is a suitable mouse model for studies into the neurobiology of rapid-acting antidepressant compounds. The majority of the published studies revealed antidepressant-like effects of ketamine 24 hours after injection (16). In addition, several studies have shown a sustained, lasting effect of ketamine up to two weeks (26). This prompted us to analyze two different time points and we could indeed show that ketamine and HNK produced both acute (4 hours) and sustained (1 week) antidepressant-like effect in male DBA/2J mice in the FST. Furthermore, ketamine administration significantly impaired locomotor activity, comparable to sedation and other related side-effects that can be prominently seen in patients (10). HNK,

in contrast, did not show an impact on locomotor activity in DBA/2J mice, supporting the fact that due to its favorable side-effects profile, HNK might be an ideal candidate to be further tested as rapid-acting antidepressant in clinical use. This prompted us to exclusively focus our in-depth proteomic analysis on HNK.

Temporal CSF proteome profiles associated with antidepressant-like effects of HNK point to involvement of GR signaling as a putative mechanism of action

As CSF is an accessible biological fluid in both mice and humans that is circulating in close vicinity to the brain, this translational approach was intended to shed light on the molecular pathways underlying HNK's rapid and sustained antidepressant-like properties. Our results demonstrated that HNK induced time-dependent changes in the murine CSF proteome compared to vehicle-treated control mice.

Our data point, for the first time, to an important role of the GR signaling pathway in the rapid and sustained antidepressant-like properties of HNK. There is convincing evidence in the literature, both from human studies and experimental models, that depression is linked to a dysfunction of the hypothalamus-pituitary-adrenal (HPA) axis, finally resulting in increased levels of circulating glucocorticoids (27). In particular, impaired GR signaling was discussed to be a key mechanism in the pathogenesis of depression (28), which is in line with the hypothesis that antidepressants reduce depressive symptoms by restoring HPA axis function (27). For example, a recent study by Arango-Lievano *et al.* showed that the disruption of GR signaling in rats induced depression-like symptoms and that GR signaling was involved in modulating antidepressant-induced neuronal plasticity needed for reversal of depression-like symptoms (29). While the close link between HPA axis activity and mechanism of action is

well established for “classical” antidepressants such as tricyclic antidepressants or serotonin reuptake inhibitors, data on a putative involvement of the stress hormone system in mediating antidepressant-like effects of prototypical rapid acting compounds is sparse. For ketamine, it was described that in addition to its antidepressant-like properties, it was able to restore HPA axis function and to normalize peripheral CORT levels in a mouse chronic stress model (30). So far, data on a putative impact of HNK on modulating GR signaling was lacking. In addition to the proteomic profiling data pointing to an involvement of GR signalling, we here provide a first mechanistic insight into HNK’s effect on GR function: we could show, for the first time, that GR responsiveness *in vitro* was reduced following HNK treatment. Interestingly, a large majority of the proteins implicated in the GR signaling are composed of keratins and these structural proteins were found to be down-regulated following HNK treatment at both time points. Although keratins are traditionally associated with the skin (31), their role in stress signaling has opened a new avenue in neurological disorders. This is supported by recent findings that provided compelling experimental evidence on the role of a specific keratin in CSF as a potential biomarker for Alzheimer’s disease (32). Furthermore, a study by Helenius et al. has lent support to the notion that the expression levels of different keratin subtypes are proportionate to stress in intestinal diseases (33). Apart from keratins, heat shock proteins (HSPs) were also found to be similarly differentially expressed in stress conditions (33). Correspondingly, our results have demonstrated that HSPA5 and HSPA9 were also downregulated in addition to the keratins at the 1w time point. Therefore, based on these results, it is tempting to suggest that downregulation of keratins and also HSPs in our mouse model reflect the HNK-mediated amelioration of stress and this effect lasted for as long as one week. Collectively, these results highlight the crucial effect of HNK in regulating the GR signaling in maintaining the homeostatic balance in the CSF proteome. Among the other differentially expressed candidate proteins, we found Dynll2 which plays a pivotal role

in controlling cytoskeletal structures (34) to be upregulated 4 hours after HNK administration. Several other cytoskeletal proteins like Arpc4, Vim, Tubb5, Klkb1, and Msn were also shown to be induced one week after HNK administration. These findings are in line with recent reports indicating the relevance of cytoskeletal dynamics in translating stressful environmental experiences into persistent changes of molecular and cellular function (35, 36). The fact that we identified a considerable number of cytoskeletal proteins to be specifically regulated by HNK (i.e. putative targets of HNK) could point to their involvement in mediating rapid antidepressant-like effects, which is an intriguing hypothesis considering their crucial role in fine-tuning of synaptic plasticity and function (37). Moreover, we found proteins Mbp, Plp1, and Psap to be altered by HNK administration, with downregulation of Mbp and Plp1 at 4 hours following HNK administration, and upregulation one week later. The latter are proteins playing important roles in myelination and myelin integrity (38). In fact, Weckmann and colleagues provided evidence that ketamine, the parent compound of HNK, increased Mbp protein levels in mice (39). In addition, the antidepressant-like effects of ketamine are known to take effect *via* enhancement of synaptogenesis: a single injection of ketamine triggered mammalian target of rapamycin (mTOR) pathway, which led to antidepressant-like effects by enhancing synaptogenesis in the medial prefrontal cortex of rodents (40-42). The bidirectional amino acid transport with SLC transporter proteins is known to regulate mTOR activation (43). Indeed, we found that mTOR was one of the top predicted upstream regulators, which was activated one week after HNK administration. Correspondingly, transporter proteins Slc25a4 and SLC25A5 were also shown to be upregulated one week after HNK administration. Collectively, these results indicate that the activation of the mTOR pathway might play a pivotal mechanistic role in mediating HNK's rapid behavioral effects, comparable to what has been described for ketamine.

A limitation of this study is that pooled CSF samples were used for the MS-based proteomics analyses. Although it has been shown that mouse CSF samples can be analyzed individually (44), we pooled the samples to minimize inter-individual variation.

In conclusion, our study substantially advances our knowledge about the molecular and cellular mechanisms through which HNK as a prototypical rapid acting antidepressant compound exerts its acute and sustained antidepressant-like effects. We could confirm the DBA/2J inbred mouse strain to be a suitable animal model for investigations into the neurobiological mechanisms underlying rapid-acting antidepressants. Our translationally relevant approach provides unprecedentedly detailed information on the temporal profile of CSF proteome changes in response to HNK. Finally, by a combination of the hypothesis-free mass spectrometry approach with candidate-driven *in vitro* experiments, we identified, for the first time, GR signaling to be a specific target of HNK. We are confident that those data can be a valuable resource for future studies investigating improved, rapid acting strategies to treat depression.

Methods

Animals

Male, adult (8 weeks) DBA/2J mice were purchased from Charles River, France. After arrival at our animal facility, we single-housed all the mice (temperature = 22±2 °C, relative humidity = 50±5 %) and allowed them to habituate to the new environment for at least one week prior to any experiments. We applied a standard 12h dark/light cycle (8am – 8pm light, 8pm – 8am dark). Mice had *ad libitum* access to water and food. All experiments were conducted in accordance with European animal welfare laws and approved by the local animal welfare authority (Landesuntersuchungsamt Rheinland-Pfalz, Koblenz, Germany).

Drug administration

Murine body weight (BW) was measured 24 h before drug administration. Mice received ketamine hydrochloride (Inresa Arzneimittel GmbH, Germany; 30 mg/kg BW, 5 mg/ml), (2*R*,6*R*)-hydroxynorketaminehydrochloride (Tocris, Germany; 10 mg/kg BW, 2.5 mg/ml), or saline control (0.9% NaCl, Braun, Germany) intraperitoneally.

Behavioral assessment

Forced Swim Test (FST)

Mice were handled for 2 minutes daily for three consecutive days. We then injected them once with either ketamine or HNK or saline. We performed the FST to assess depressive-like behavior 4 h and 1 week after injection. Mice were introduced into a 2-L glass beaker (diameter 13 cm, height 24 cm) filled with tap water (21±1 °C) to a height of 15 cm. We videotaped the mice for 5 minutes and floating, swimming, and struggling behavior was scored by an experienced, observer blinded towards the treatment.

Open Field Test (OF)

In a new and independent experiment, mice were handled for 2 minutes daily for three consecutive days. We then injected them once with either ketamine or HNK or saline and immediately placed them into the OF arena (45x45x41 cm). We performed the OF to assess locomotor activity. Mice could move freely and without disturbance for 30 minutes, during which they were videotaped from above. Distanced moved was automatically scored with the tracking software Observer XT12 (Noldus, The Netherlands).

Blood plasma extraction

We withdrew blood *via* tail nicks into EDTA-coated tubes, as previously described (45). We centrifuged all tubes for 10 min at 10 000 *g* at 4 °C and stored the plasma at -80 °C until further use.

Corticosterone (CORT) plasma concentration

We measured CORT plasma levels using the Corticosterone ELISA Kit (cat.no. ADI-900-0979; Enzo Life Sciences, USA) according to the manufacturer´s protocol in duplicates.

Statistics of behavioral experiments and neuroendocrine measurements

Data was plotted and descriptive statistics were applied to check for normal distribution of the data (D'Agostino & Pearson omnibus normality test). We analyzed data with a 1- or 2-way ANOVA followed by Bonferroni correction. Alpha was set at 5%, with p values <0.05 considered statistically significant. Data was analyzed using Prism 5 software (GraphPad, USA). Sample sizes are indicated in the figure legends. The values are displayed as mean ± SEM.

CSF cannula surgery

Ketamine and HNK were equally effective with respect to their antidepressant-like efficacy. Due to the improved side-effect profile of HNK and the gap of knowledge about the neurobiological mechanisms mediating its antidepressant-like activity, we exclusively focused on HNK with respect to the proteome profiling of the CSF.

CSF cannula implantation was conducted in a modified way based on the method by Onaivi and colleagues (19). In brief, mice were anesthetized with Isoflurane (Forene®, AbbVie Deutschland GmbH, Germany) and received the analgesic drug Metacam (Boehringer Ingelheim Vetmedica GmbH, Germany) subcutaneously (0.5 mg/kg BW). The skin was opened and two small holes were drilled into the skull, followed by applying two screws. A third hole was drilled and the intraventricular cannula (internal cannula; Plastics One, USA) was implanted at bregma coordinates 0.0 AP / 0.8 ML / -0.9 VD. Paladur dental cement (Kulzer, Germany) was used to secure the internal cannula to the screws and the skull. The skin lesion was closed and a dummy cannula (Plastics One, USA) closed the internal cannula. Subsequently, the mice received Metacam in the drinking water for one week. After recovery from surgery, mice received new water bottles without the analgesic drug.

CSF withdrawal and protocol of the main experiment

Mice were handled carefully for 2 minutes per day for 1 week. CSF was withdrawn from all mice and the first sample was discarded to exclude contamination with blood. After three days, mice were randomized into an HNK or saline arm (Supplemental data A). They received an intraperitoneal injection of either HNK or saline and CSF samples were taken 4 hours and 1 week after injection.

CSF withdrawals were conducted as follows: Dummy cannula was removed and tubing (5-10cm in length; Plastics One, USA) with external cannula (additional -1.0 VD (final depth -

1.9 VD); Plastics One, USA) was connected to the internal of the cannula at one end and to a 10µl Model 701 N Hamilton syringe (cat.no. 80365; Hamilton, USA) at the other end. By gently pulling the plunger in steps of 1µl for each 1 minute, CSF was withdrawn. After the plunger reached 10µl, CSF was collected and directly put on dry ice and later stored at -80°C until further analyses. CSF-containing tubes were visually inspected for any blood contamination and excluded if necessary.

Proteomics sample preparation

The obtained CSF samples of the designated groups were pooled with three biological replicates each, as described in supplemental data A. Briefly, the CSF samples in each assigned biological replicate were pooled equally to a total of 40 µl per replicate. The designated samples were then subjected to one-dimensional gel electrophoresis (1DE) employing precast NuPAGE 4-12% Bis-Tris 10-well mini protein gels (Invitrogen, Germany) with 2-[N-morpholino]ethanesulfonic acid (MOPS) running buffer under reducing conditions at a constant voltage of 150V in 4 °C. Pre-stained protein standard, SeeBlue Plus 2 (Invitrogen, Germany), was used as a molecular mass marker and the gels were stained with Colloidal Blue Staining Kit (Invitrogen, Germany), as per manufacturer's instructions. The bands in each stained gel were sliced into 14 gel slices per lane with the aim to reduce the complexity and masking effect of the abundant proteins during the MS analysis (Supplemental figure 2). Protein bands were excised (14 bands per replicate) Subsequently, all the excised protein bands were destained, reduced and alkylated prior to in-gel trypsin digestion employing sequence grade-modified trypsin (Promega, USA), as described in detail elsewhere (46-48). Peptides extracted from trypsin digestion were purified with ZipTip C18 pipette tips (Millipore, Billerica, MA, USA) according to the manufacturer's instructions. The resulting combined peptide eluate was concentrated to dryness in a centrifugal vacuum

evaporator (SpeedVac) and dissolved in 10 µl of 0.1% trifluoroacetic acid (TFA) for liquid chromatography-electrospray ionization-tandem mass spectrometry (LC-ESI-MS/MS) analysis.

Discovery proteomics strategy

Peptide fractionation was conducted in the LC system, which consisted of a Rheos Allegro pump (Thermo Scientific, USA) and an HTS PAL autosampler (CTC Analytics AG, Switzerland) equipped with a BioBasic C18, 30 x 0.5 mm precolumn (Thermo Scientific, USA) connected to a BioBasic C18, 150 x 0.5 mm analytical column (Thermo Scientific, USA). Solvent A consisted of LC-MS grade water with 0.1 % (v/v) formic acid and solvent B was LC-MS grade acetonitrile with 0.1 % (v/v) formic acid. The gradient was run for 60 min per sample as follows: 0-35 min: 15-40 % B, 35-40 min: 40-60 % B, 40-45 min: 60-90 % B, 45-50 min: 90 % B, 50-53 min: 90-10 % B: 53-60 min: 10 % B.

The continuum MS data were obtained on an ESI-LTQ Orbitrap XL-MS system (Thermo Scientific, Bremen, Germany). The general parameters of the instrument were set as follows: positive ion electrospray ionization mode, a spray voltage of 2.15 KV and a heated capillary temperature of 220 ºC. Data was acquired in an automatic dependent mode whereby, there was automatic acquisition switching between Orbitrap-MS and LTQ MS/MS. The Orbitrap resolution was 30000 at *m/z* 400 with survey full scan MS spectra ranging from an m/z of 300 to 1600. Target automatic gain control (AGC) was set at 1.0 x 10^6 ion. Internal recalibration employed polydimethlycyclosiloxane (PCM) at m/z 445.120025 ions in real time and the lock mass option was enabled in MS mode (49). Tandem data was obtained by selecting top five most intense precursor ions and subjected them for further fragmentation by collision-induced dissociation (CID). The normalized collision energy (NCE) was set to 35 % with activation time of 30 ms with repeat count of three and dynamic exclusion duration of 600 s.

The resulting fragmented ions were recorded in the LTQ. The acquired continuum MS spectra were analyzed by MaxQuant computational proteomics platform version 1.6.3.3 and its built-in Andromeda search engine for peptide and protein identification (50-54). The tandem MS spectra were searched against UniProt *Homo sapiens* (Date, 17 Oct 2018; 20 410 proteins listed) and *Mus musculus* (Date, 17 Oct 2018; 17 001 proteins listed) databases, using standard settings with peptide mass tolerance of ± 30 ppm, fragment mass tolerance of ±0.5 Da, with ≥ 6 amino acid residues and only "unique plus razor peptides" that belong to a protein were chosen (51). Both the *Mus musculus* and *Homo sapiens* databases were utilized with the aim to maximize the protein identification due to limited availability of annotated mouse proteins in a specific database (47). A target-decoy-based false discovery rate (FDR) for peptide and protein identification was set to 0.01. Carbamidomethylation of cysteine was set as a fixed modification, while protein N-terminal acetylation and oxidation of methionine were defined as variable modifications, enzyme: trypsin and maximum number of missed cleavages: 2. The generated MaxQuant output data table "proteingroups.txt" was filtered for reverse hits prior to statistical analysis and, subsequent functional annotation and pathway analyses. The summary of MaxQuant parameters employed in the current analyses is tabulated in Supplemental data B.

Bioinformatics and functional annotation and pathways analyses

The output of the generated "proteingroups.txt" data from the MaxQuant analysis was utilized for subsequent statistical analysis with Perseus software (version1.6.1.3). First, all raw intensities were $\log_2$-transformed and the data were filtered with minimum of three valid values in at least one group and the missing values were imputated by replacing from normal distribution (width: 0.3; down shift: 1.8)), enabling statistical analysis (54). For statistical evaluation, a two-sided Student's t-test was used for the group comparison with p-values <

0.05 to identify the significantly differentially abundant proteins. Unsupervised hierarchical clustering analysis of the differentially expressed proteins was conducted with $\log_2$ fold ratio of the protein intensities according to Euclidean distance (linkage = average; preprocess with k-means) and elucidated in a heat map. The overlaps of the statistically differentially expressed proteins between the databases utilized were manually curated based on the highest significance values. The list of the identified proteins was tabulated in Excel and their gene names were used for subsequent functional annotation and pathways analyses employing Ingenuity Pathway Analysis (v01-04, IPA; Ingenuity QIAGEN Redwood City, CA) (https://www.qiagenbioinformatics.com/products/ingenuity-pathway-analysis) (55). IPA analyses unraveled the protein-protein interaction (PPI) networks, identified the significantly affected canonical pathways, top disease and functions, and predicted upstream regulators associated with the proteins identified to be differentially expressed. Top canonical pathways of the differentially expressed proteins were presented with p-value calculated using Benjamini-Hochberg (B-H) multiple testing correction (–log B-H > 1.3) and a cut-off of ≥ 3 affected proteins per pathway. In PPI networks, proteins molecules are represented by their corresponding gene names and, only PPIs that were experimentally observed and had direct and indirect interactions were used.

In vitro GR activity and gene reporter assays

HT-22 mouse hippocampal neuronal cell line was used as an in vitro model to analyze the molecular effects of HNK on GR transcriptional activity and GR sensitivity to glucocorticoids. Experiments were conducted as described before (56, 57). Briefly, cells were cultivated, transfected with MMTV-Luc and Gaussia-Luc expression constructs using Lipofectamine 2000 (Thermofisher) and treated with HNK in concentrations of 0.1 µM, 1.0 µM, 10.0 µM, and 30.0 µM. Two conditions using culture medium (DMEM, Gibco)

supplemented with either standard fetal bovine serum as or with charcoal stripped serum as steroid-free condition were examined to observe HNK effects on the GR-driven transcriptional activity. For evaluating the GR response to hormonal activation, GR-agonist dexamethasone (0.1 nM, 0.3 nM, 1 nM, 3 nM, 10 nM, 30 nM, 100 nM) was added and cells were treated with either HNK (5µM) or vehicle. Data were analyzed using 2-way ANOVA followed by Bonferroni correction. Alpha was set at 5%, with $p < 0.05$ considered statistically significant. Data was analyzed using Prism 5 software (GraphPad, USA).

Author Contributions

DH, NP, MM designed the research. DH, GT, JN, JE, TJ, AH, and MvdK performed animal experiments. NP, CM, MR performed proteomics experiments. NG performed in vitro experiments. DH, NP, CM, and NG analyzed the data. All authors made a substantial contribution to the interpretation of the data and to the drafting of the manuscript. DH and NP shared first authorship and are listed in alphabetical order.

Acknowledgements

We are thankful for the technical support by Kathrin Kuna (Mainz, Germany). A portion of the work described herein was carried out by Jens Nadig and Milena Rossmanith in partial fulfilment of the requirements for a medical doctoral degree at the Johannes Gutenberg University Medical Center Mainz, Germany.

DH is supported by the Mainz Research School of Translational Biomedicine (TransMed) with a MD-PhD fellowship. CM is supported by the German Research Foundation (DFG), grant number MA 8006/1-1. TJ is supported by the Focus Program of Translational Neurosciences (FTN) in Mainz with a PhD fellowship. GT is supported by a 2014 NARSAD Young Investigator Grant from the Brain & Behavior Research Foundation and the Danish Council for Independent Research, grant number DFF-5053-00103. MM and KL are supported by the German Research Foundation (DFG) within the Collaborative Research Center 1193 (CRC1193, https://crc1193.de/) and by the Boehringer Ingelheim Foundation.

References

1. Johnston KM, Powell LC, Anderson IM, Szabo S, and Cline S. The burden of treatment-resistant depression: A systematic review of the economic and quality of life literature. *Journal of affective disorders.* 2019;242:195-210.
2. Dong M, Zeng LN, Lu L, Li XH, Ungvari GS, Ng CH, et al. Prevalence of suicide attempt in individuals with major depressive disorder: a meta-analysis of observational surveys. *Psychol Med.* 2019;49(10):1691-704.
3. Sobocki P, Jonsson B, Angst J, and Rehnberg C. Cost of depression in Europe. *The journal of mental health policy and economics.* 2006;9(2):87-98.
4. Labermaier C, Masana M, and Muller MB. Biomarkers predicting antidepressant treatment response: how can we advance the field? *Disease markers.* 2013;35(1):23-31.
5. Lener MS, Kadriu B, and Zarate CA, Jr. Ketamine and Beyond: Investigations into the Potential of Glutamatergic Agents to Treat Depression. *Drugs.* 2017;77(4):381-401.
6. Berman RM, Cappiello A, Anand A, Oren DA, Heninger GR, Charney DS, et al. Antidepressant effects of ketamine in depressed patients. *Biological psychiatry.* 2000;47(4):351-4.
7. Browne CA, and Lucki I. Antidepressant effects of ketamine: mechanisms underlying fast-acting novel antidepressants. *Frontiers in pharmacology.* 2013;4:161.
8. Schwartz J, Murrough JW, and Iosifescu DV. Ketamine for treatment-resistant depression: recent developments and clinical applications. *Evid Based Ment Health.* 2016;19(2):35-8.
9. Cavalleri L, Merlo Pich E, Millan MJ, Chiamulera C, Kunath T, Spano PF, et al. Ketamine enhances structural plasticity in mouse mesencephalic and human iPSC-derived dopaminergic neurons via AMPAR-driven BDNF and mTOR signaling. *Molecular psychiatry.* 2018;23(4):812-23.
10. Short B, Fong J, Galvez V, Shelker W, and Loo CK. Side-effects associated with ketamine use in depression: a systematic review. *The lancet Psychiatry.* 2018;5(1):65-78.
11. Chou D, Peng HY, Lin TB, Lai CY, Hsieh MC, Wen YC, et al. (2R,6R)-hydroxynorketamine rescues chronic stress-induced depression-like behavior through its actions in the midbrain periaqueductal gray. *Neuropharmacology.* 2018;139:1-12.
12. Pham TH, Defaix C, Xu X, Deng SX, Fabresse N, Alvarez JC, et al. Common Neurotransmission Recruited in (R,S)-Ketamine and (2R,6R)-Hydroxynorketamine-Induced Sustained Antidepressant-like Effects. *Biological psychiatry.* 2018;84(1):e3-e6.
13. Zanos P, Moaddel R, Morris PJ, Georgiou P, Fischell J, Elmer GI, et al. NMDAR inhibition-independent antidepressant actions of ketamine metabolites. *Nature.* 2016;533(7604):481-6.
14. Lumsden EW, Troppoli TA, Myers SJ, Zanos P, Aracava Y, Kehr J, et al. Antidepressant-relevant concentrations of the ketamine metabolite (2R,6R)-hydroxynorketamine do not block NMDA receptor function. *Proceedings of the National Academy of Sciences of the United States of America.* 2019;116(11):5160-9.
15. Zanos P, Thompson SM, Duman RS, Zarate CA, Jr., and Gould TD. Convergent Mechanisms Underlying Rapid Antidepressant Action. *CNS drugs.* 2018;32(3):197-227.
16. Herzog DP, Wegener G, Lieb K, Muller MB, and Treccani G. Decoding the Mechanism of Action of Rapid-Acting Antidepressant Treatment Strategies: Does Gender Matter? *International journal of molecular sciences.* 2019;20(4).
17. NICE. Depression in adults: recognition and management - National Institute for Health and Care Excellence guidelines [CG90]. www.nice.org.uk/guidance/cg90. Accessed 02 January 2019.

18. Carrillo-Roa T, Labermaier C, Weber P, Herzog DP, Lareau C, Santarelli S, et al. Common genes associated with antidepressant response in mouse and man identify key role of glucocorticoid receptor sensitivity. *PLoS Biol.* 2017;15(12):e2002690.
19. Onaivi ES, Schanz N, and Lin ZC. Psychiatric disturbances regulate the innate immune system in CSF of conscious mice. *Translational psychiatry.* 2014;4:e367.
20. Sillaber I, Panhuysen M, Henniger MS, Ohl F, Kuhne C, Putz B, et al. Profiling of behavioral changes and hippocampal gene expression in mice chronically treated with the SSRI paroxetine. *Psychopharmacology.* 2008;200(4):557-72.
21. Sugimoto Y, Yamamoto M, Tagawa N, Kobayashi Y, Mitsui-Saitoh K, Hotta Y, et al. Differences between mice strains in response to paroxetine in the forced swimming test: involvement of serotonergic or noradrenergic systems. *European journal of pharmacology.* 2011;672(1-3):121-5.
22. Thoeringer CK, Sillaber I, Roedel A, Erhardt A, Mueller MB, Ohl F, et al. The temporal dynamics of intrahippocampal corticosterone in response to stress-related stimuli with different emotional and physical load: an in vivo microdialysis study in C57BL/6 and DBA/2 inbred mice. *Psychoneuroendocrinology.* 2007;32(6):746-57.
23. Gentsch C, Lichtsteiner M, and Feer H. Locomotor activity, defecation score and corticosterone levels during an openfield exposure: a comparison among individually and group-housed rats, and genetically selected rat lines. *Physiology & behavior.* 1981;27(1):183-6.
24. Fitzgerald PJ, Yen JY, and Watson BO. Stress-sensitive antidepressant-like effects of ketamine in the mouse forced swim test. *PloS one.* 2019;14(4):e0215554.
25. Yamaguchi JI, Toki H, Qu Y, Yang C, Koike H, Hashimoto K, et al. (2R,6R)-Hydroxynorketamine is not essential for the antidepressant actions of (R)-ketamine in mice. *Neuropsychopharmacology : official publication of the American College of Neuropsychopharmacology.* 2018;43(9):1900-7.
26. Brachman RA, McGowan JC, Perusini JN, Lim SC, Pham TH, Faye C, et al. Ketamine as a Prophylactic Against Stress-Induced Depressive-like Behavior. *Biological psychiatry.* 2016;79(9):776-86.
27. Anacker C, Zunszain PA, Carvalho LA, and Pariante CM. The glucocorticoid receptor: pivot of depression and of antidepressant treatment? *Psychoneuroendocrinology.* 2011;36(3):415-25.
28. Holsboer F. The corticosteroid receptor hypothesis of depression. *Neuropsychopharmacology : official publication of the American College of Neuropsychopharmacology.* 2000;23(5):477-501.
29. Arango-Lievano M, Lambert WM, Bath KG, Garabedian MJ, Chao MV, and Jeanneteau F. Neurotrophic-priming of glucocorticoid receptor signaling is essential for neuronal plasticity to stress and antidepressant treatment. *Proceedings of the National Academy of Sciences of the United States of America.* 2015;112(51):15737-42.
30. Wang W, Liu L, Yang X, Gao H, Tang QK, Yin LY, et al. Ketamine improved depressive-like behaviors via hippocampal glucocorticoid receptor in chronic stress induced- susceptible mice. *Behavioural brain research.* 2019;364:75-84.
31. Toivola DM, Boor P, Alam C, and Strnad P. Keratins in health and disease. *Curr Opin Cell Biol.* 2015;32:73-81.
32. Richens JL, Spencer HL, Butler M, Cantlay F, Vere KA, Bajaj N, et al. Rationalising the role of Keratin 9 as a biomarker for Alzheimer's disease. *Scientific reports.* 2016;6:22962.
33. Helenius TO, Antman CA, Asghar MN, Nystrom JH, and Toivola DM. Keratins Are Altered in Intestinal Disease-Related Stress Responses. *Cells.* 2016;5(3).
34. Rapali P, Szenes A, Radnai L, Bakos A, Pal G, and Nyitray L. DYNLL/LC8: a light chain subunit of the dynein motor complex and beyond. *FEBS J.* 2011;278(17):2980-96.

35. Kretzschmar A, Schulke JP, Masana M, Durre K, Muller MB, Bausch AR, et al. The Stress-Inducible Protein DRR1 Exerts Distinct Effects on Actin Dynamics. *International journal of molecular sciences.* 2018;19(12).
36. van der Kooij MA, Masana M, Rust MB, and Muller MB. The stressed cytoskeleton: How actin dynamics can shape stress-related consequences on synaptic plasticity and complex behavior. *Neurosci Biobehav Rev.* 2016;62:69-75.
37. Cingolani LA, and Goda Y. Actin in action: the interplay between the actin cytoskeleton and synaptic efficacy. *Nature reviews Neuroscience.* 2008;9(5):344-56.
38. Campagnoni AT, and Skoff RP. The pathobiology of myelin mutants reveal novel biological functions of the MBP and PLP genes. *Brain Pathol.* 2001;11(1):74-91.
39. Weckmann K, Deery MJ, Howard JA, Feret R, Asara JM, Dethloff F, et al. Ketamine's Effects on the Glutamatergic and GABAergic Systems: A Proteomics and Metabolomics Study in Mice. *Mol Neuropsychiatry.* 2019;5(1):42-51.
40. Casarotto PC, Girych M, Fred SM, Kovaleva V, Moliner R, Enkavi G, et al. Antidepressant drugs act by directly binding to TRKB neurotrophin receptors. *Cell.* 2021;184(5):1299-313 e19.
41. Li N, Lee B, Liu RJ, Banasr M, Dwyer JM, Iwata M, et al. mTOR-dependent synapse formation underlies the rapid antidepressant effects of NMDA antagonists. *Science.* 2010;329(5994):959-64.
42. Li N, Liu RJ, Dwyer JM, Banasr M, Lee B, Son H, et al. Glutamate N-methyl-D-aspartate receptor antagonists rapidly reverse behavioral and synaptic deficits caused by chronic stress exposure. *Biological psychiatry.* 2011;69(8):754-61.
43. Nicklin P, Bergman P, Zhang B, Triantafellow E, Wang H, Nyfeler B, et al. Bidirectional transport of amino acids regulates mTOR and autophagy. *Cell.* 2009;136(3):521-34.
44. Smith JS, Angel TE, Chavkin C, Orton DJ, Moore RJ, and Smith RD. Characterization of individual mouse cerebrospinal fluid proteomes. *Proteomics.* 2014;14(9):1102-6.
45. van der Kooij MA, Jene T, Treccani G, Miederer I, Hasch A, Voelxen N, et al. Chronic social stress-induced hyperglycemia in mice couples individual stress susceptibility to impaired spatial memory. *Proceedings of the National Academy of Sciences of the United States of America.* 2018;115(43):E10187-E96.
46. Manicam C, Perumal N, Wasielica-Poslednik J, Ngongkole YC, Tschabunin A, Sievers M, et al. Proteomics Unravels the Regulatory Mechanisms in Human Tears Following Acute Renouncement of Contact Lens Use: A Comparison between Hard and Soft Lenses. *Scientific reports.* 2018;8(1):11526.
47. Perumal N, Strassburger L, Herzog DP, Muller MB, Pfeiffer N, Grus FH, et al. Bioenergetic shift and actin cytoskeleton remodelling as acute vascular adaptive mechanisms to angiotensin II in murine retina and ophthalmic artery. *Redox Biol.* 2020:101597.
48. Perumal N, Strassburger L, Schmelter C, Gericke A, Pfeiffer N, Grus FH, et al. Sample Preparation for Mass-spectrometry-based Proteomics Analysis of Ocular Microvessels. *Journal of visualized experiments : JoVE.* 2019(144).
49. Olsen JV, de Godoy LM, Li G, Macek B, Mortensen P, Pesch R, et al. Parts per million mass accuracy on an Orbitrap mass spectrometer via lock mass injection into a C-trap. *Molecular & cellular proteomics : MCP.* 2005;4(12):2010-21.
50. Cox J, Hein MY, Luber CA, Paron I, Nagaraj N, and Mann M. Accurate proteome-wide label-free quantification by delayed normalization and maximal peptide ratio extraction, termed MaxLFQ. *Molecular & cellular proteomics : MCP.* 2014;13(9):2513-26.
51. Cox J, and Mann M. MaxQuant enables high peptide identification rates, individualized p.p.b.-range mass accuracies and proteome-wide protein quantification. *Nature biotechnology.* 2008;26(12):1367-72.

52. Cox J, Neuhauser N, Michalski A, Scheltema RA, Olsen JV, and Mann M. Andromeda: a peptide search engine integrated into the MaxQuant environment. *J Proteome Res.* 2011;10(4):1794-805.
53. Luber CA, Cox J, Lauterbach H, Fancke B, Selbach M, Tschopp J, et al. Quantitative proteomics reveals subset-specific viral recognition in dendritic cells. *Immunity.* 2010;32(2):279-89.
54. Tyanova S, Temu T, and Cox J. The MaxQuant computational platform for mass spectrometry-based shotgun proteomics. *Nature protocols.* 2016;11(12):2301-19.
55. Kramer A, Green J, Pollard J, Jr., and Tugendreich S. Causal analysis approaches in Ingenuity Pathway Analysis. *Bioinformatics.* 2014;30(4):523-30.
56. Schulke JP, Wochnik GM, Lang-Rollin I, Gassen NC, Knapp RT, Berning B, et al. Differential impact of tetratricopeptide repeat proteins on the steroid hormone receptors. *PloS one.* 2010;5(7):e11717.
57. Touma C, Gassen NC, Herrmann L, Cheung-Flynn J, Bull DR, Ionescu IA, et al. FK506 binding protein 5 shapes stress responsiveness: modulation of neuroendocrine reactivity and coping behavior. *Biological psychiatry.* 2011;70(10):928-36.

Figures and figures' legends

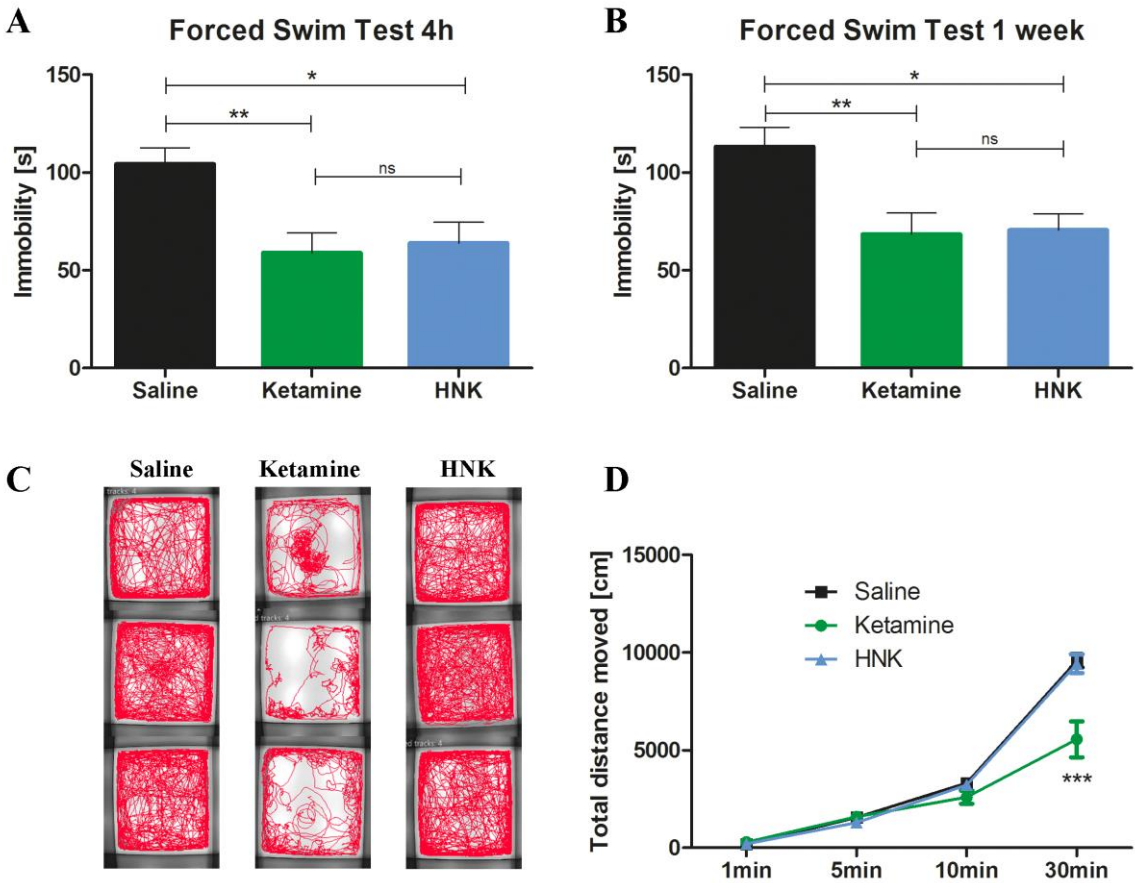

Figure 1 – Antidepressant-like effects and side-effects of ketamine and HNK. (A) 4 hours after injection, ketamine [t=3.32, p<0.01] and HNK [t=2.96, p<0.05] reduced immobility time in the FST [F=7.44, p=0.0019, n=10 per group]. (B) 1 week after injection, ketamine [t=3.24, p<0.01] and HNK [t=3.08, p<0.05] reduced immobility time in the FST [F=6.67, p=0.0044, n = 10 per group]. (C+D) Ketamine affected locomotor activity [n=10 per group]. (C) Ketamine-treated mice show an altered tracking profile [3 examples per group]. (D) Ketamine decreased locomotor activity [Interaction: F=13.32, p<0.001; time: F=388.8, p<0.001; treatment: F=7.65, p<0.01] compared to HNK [t=7.79, p<0.001] and saline [t=8.10, p<0.001]. ns not statistically significant, HNK (2R,6R)-hydroxynorketamine, * p<0.05, ** p<0.01, *** p<0.001, bars are depicted as mean ± SEM, one-way ANOVA with Bonferroni posttest in A+B, two-way repeated-measures ANOVA with Bonferroni posttest in D.

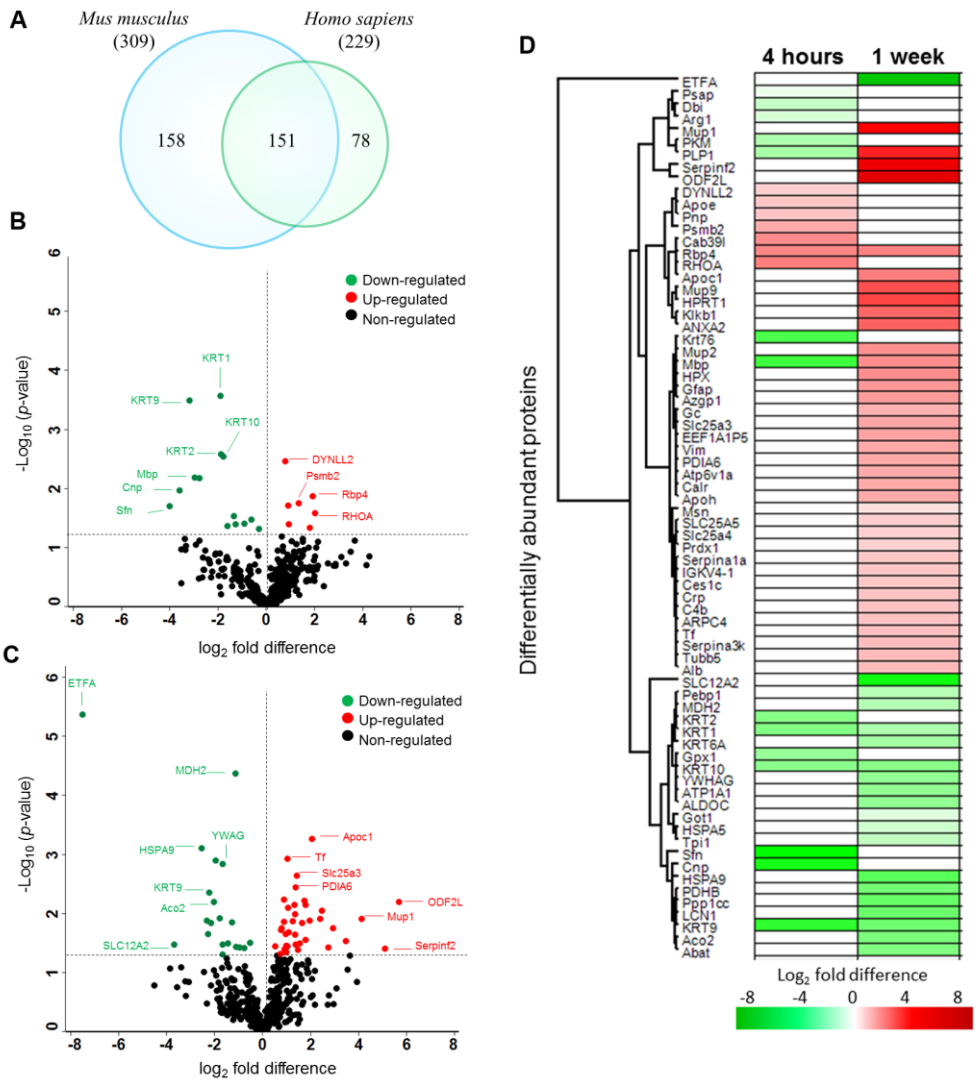

Figure 2 – Acute and sustained effects of HNK on CSF proteome. (A) Venn diagram depicts the total number of proteins identified in both mouse and human databases in the CSF samples. Volcano plot illustrates significantly differentially abundant CSF proteins after (B) 4 hours and (C) 1 week HNK administration compared to saline. The negative log10 (p-value) is plotted against the log2 (fold change: HNK/ saline). The non-axial horizontal line denotes p = 0.05, which is our significance threshold (prior to logarithmic transformation). Significantly upregulated proteins are plotted in red, while proteins that were downregulated by HNK are represented in green. (D) The hierarchical clustering of the differentially expressed CSF proteins at 4 hours and 1 week after HNK treatment displayed in a heat map. The upregulated proteins are shown in red and the downregulated proteins are in green, with $\log_2$ fold change regulation of intensity displayed in color (from -8 (green) to 8 (red).

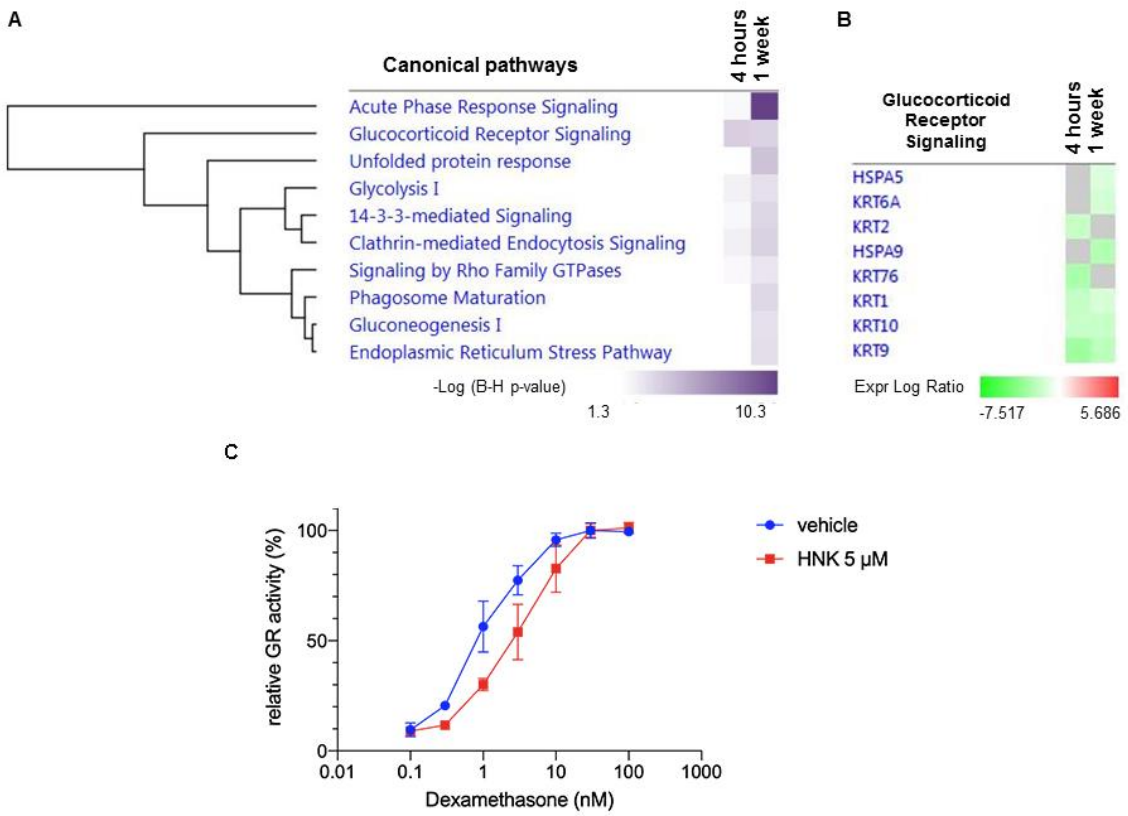

Figure 3 - Top enriched canonical pathways of the differentially expressed proteins significantly affected by HNK treatment. (A) The significantly enriched canonical pathways determined by IPA's default threshold [-log (p-value) >1.3] between the differentially expressed proteins identified in our datasets and the molecules in the respective pathways at 4h and 1w time-points following HNK treatment. (B) Proteins associated with glucocorticoid receptor signaling pathway and their expression profiles at 4 h and 1 w. The intensity of the color (green) indicates the degree of downregulation of each protein. (C) Relative GR activity was reduced through HNK (5 µM) treatment compared to vehicle control administration ($p < 0.05$ for 1.0 nM dexamethasone treatment). Relative receptor activity represents firefly luciferase activity (MMTV-promoter) normalized to Gaussia luciferase activity and is represented to the activity at saturating 30 nM dexamethasone. 2-way ANOVA followed by Bonferroni correction was applied.

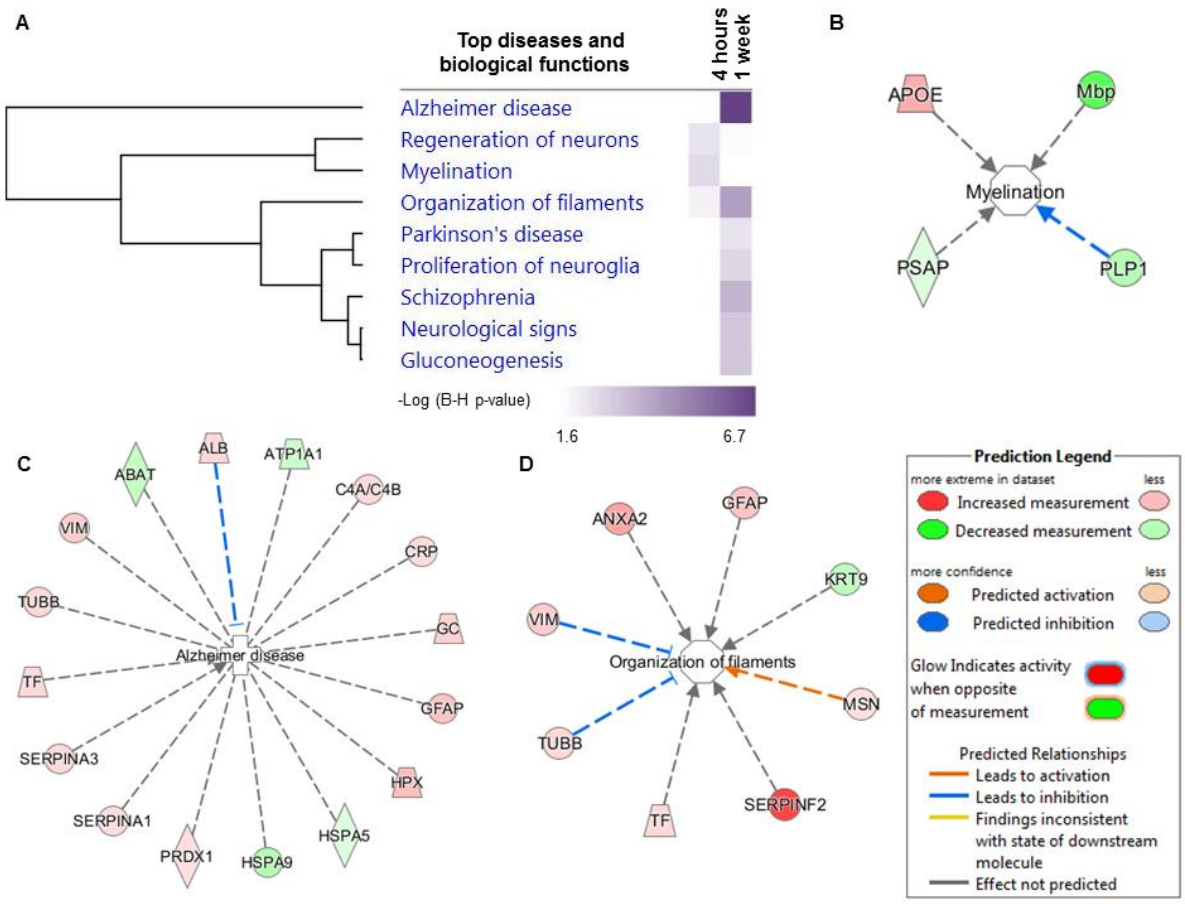

Figure 4 - Functional classification of the differentially expressed CSF proteins according to the enriched top diseases and biological functions. (A) Comparison analysis of the significantly affected diseases and biological functions between both time-points following HNK administration. The significance threshold [-log (p-value) >1.6] was determined by IPA analysis. Exemplary interaction networks of top functions at 4h represented by (B) myelination and at 1w represented by (C) Alzheimer's disease as well as (D) organization of filaments.

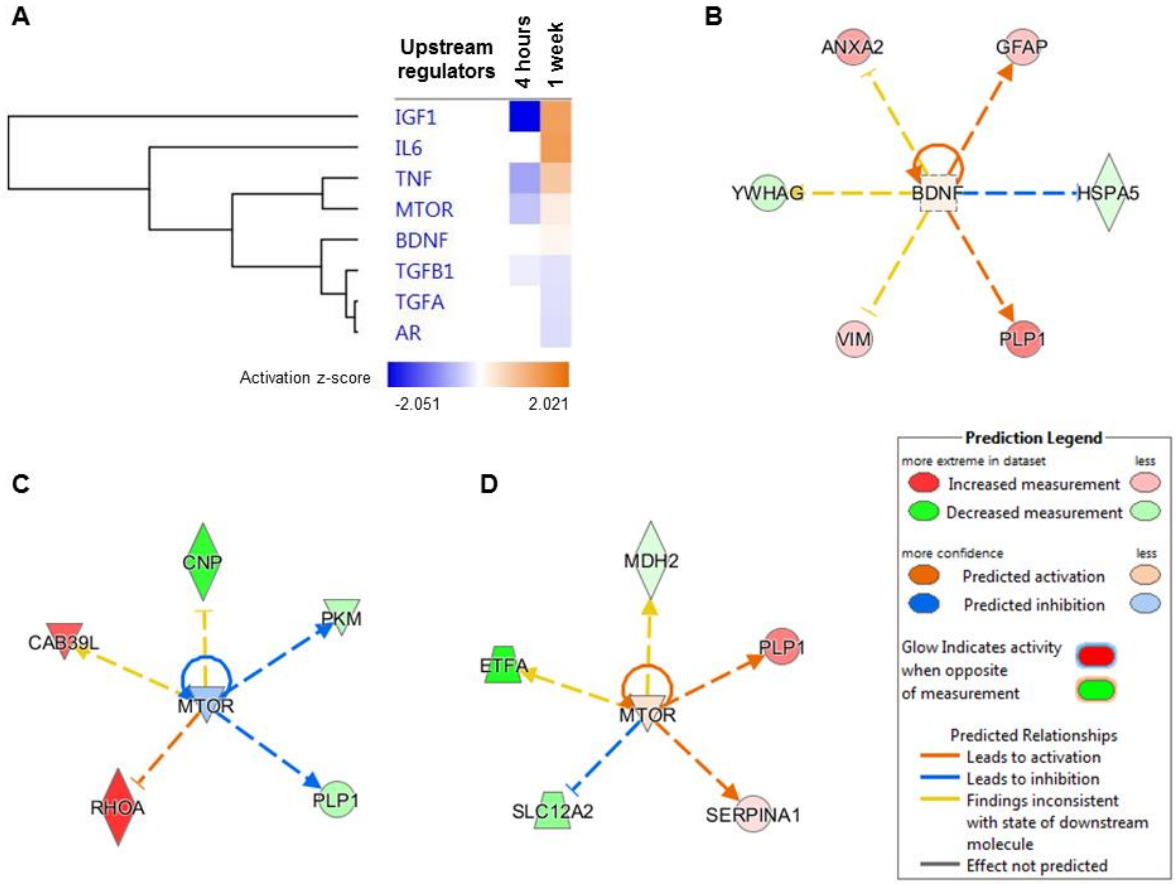

Figure 5 - Predicted upstream regulators. (A) Hierarchical clustering of the significantly affected potential upstream regulators observed to experimentally affect the differentially expressed CSF protein clusters at 4h and 1w. The activation z-score of the regulators is depicted as orange (activated) and blue (inhibited). Interaction networks that exemplify the top regulators composed of (B) brain-derived neurotrophic factor (BDNF) and the regulation of mechanistic target of rapamycin (mTOR) at (C) 4h and (D) 1w.

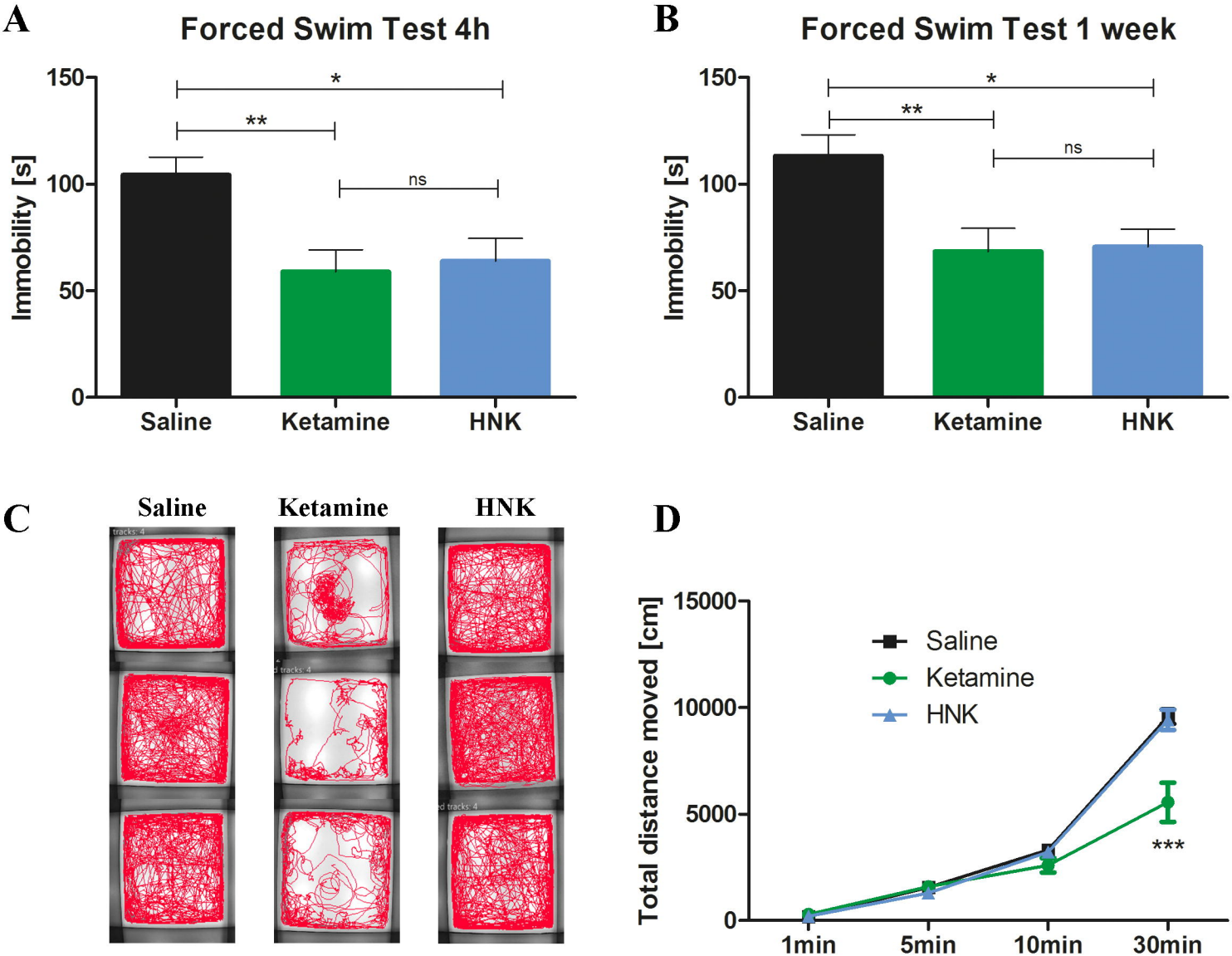
A
Forced Swim Test 4h
Immobility [s]
150
100
50
0
*
**
ns
Saline
Ketamine
HNK
B
Forced Swim Test 1 week
Immobility [s]
150
100
50
0
*
**
ns
Saline
Ketamine
HNK
C
Saline
Ketamine
HNK
D
Total distance moved [cm]
15000
10000
5000
0
Saline
Ketamine
HNK
***
1min
5min
10min
30min

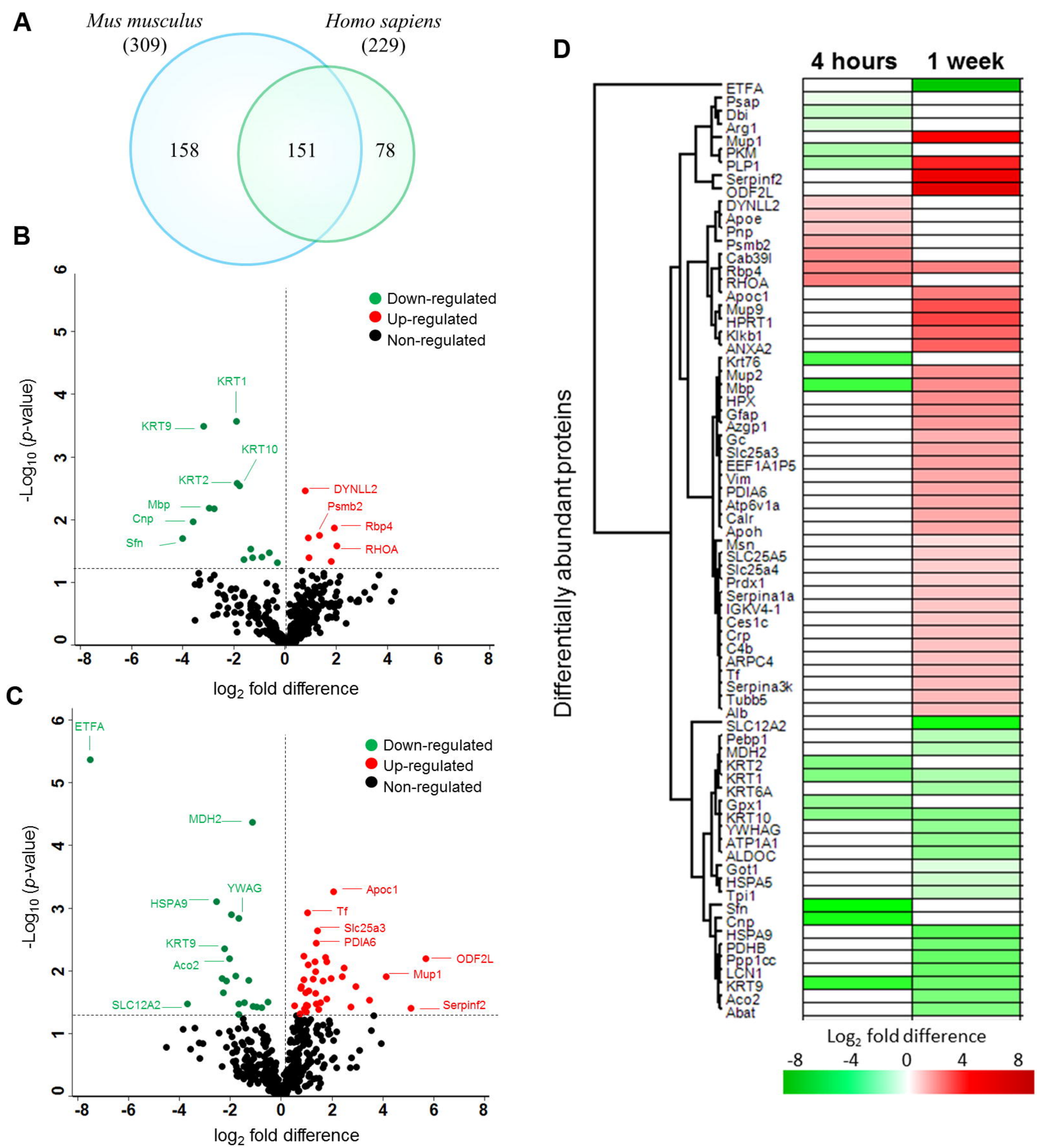
A
Mus musculus
(309)
Homo sapiens
(229)
158
151
78
B
Down-regulated
Up-regulated
Non-regulated
KRT1
KRT9
KRT10
KRT2
Mbp
Cnp
Sfn
DYNLL2
Psmb2
Rbp4
RHOA
-Log10 (p-value)
log2 fold difference
C
ETFA
MDH2
YWAG
HSPA9
KRT9
Aco2
SLC12A2
Apoc1
Tf
Slc25a3
PDIA6
ODF2L
Mup1
Serpinf2
D
4 hours
1 week
Differentially abundant proteins
ETFA
Psap
Dbi
Arg1
Mup1
PKM
PLP1
Serpinf2
ODF2L
DYNLL2
Apoe
Pnp
Psmb2
Cab39l
Rbp4
RHOA
Apoc1
Mup9
HPRT1
Klkb1
ANXA2
Krt76
Mup2
Mbp
HPX
Gfap
Azgp1
Gc
Slc25a3
EEF1A1P5
Vim
PDIA6
Atp6v1a
Calr
Apoh
Msn
SLC25A5
Slc25a4
Prdx1
Serpina1a
IGKV4-1
Ces1c
Crp
C4b
ARPC4
Tf
Serpina3k
Tubb5
Alb
SLC12A2
Pebp1
MDH2
KRT2
KRT1
KRT6A
Gpx1
KRT10
YWHAG
ATP1A1
ALDOC
Got1
HSPA5
Tpi1
Sfn
Cnp
HSPA9
PDHB
Ppp1cc
LCN1
KRT9
Aco2
Abat
Log2 fold difference
-8
-4
0
4
8

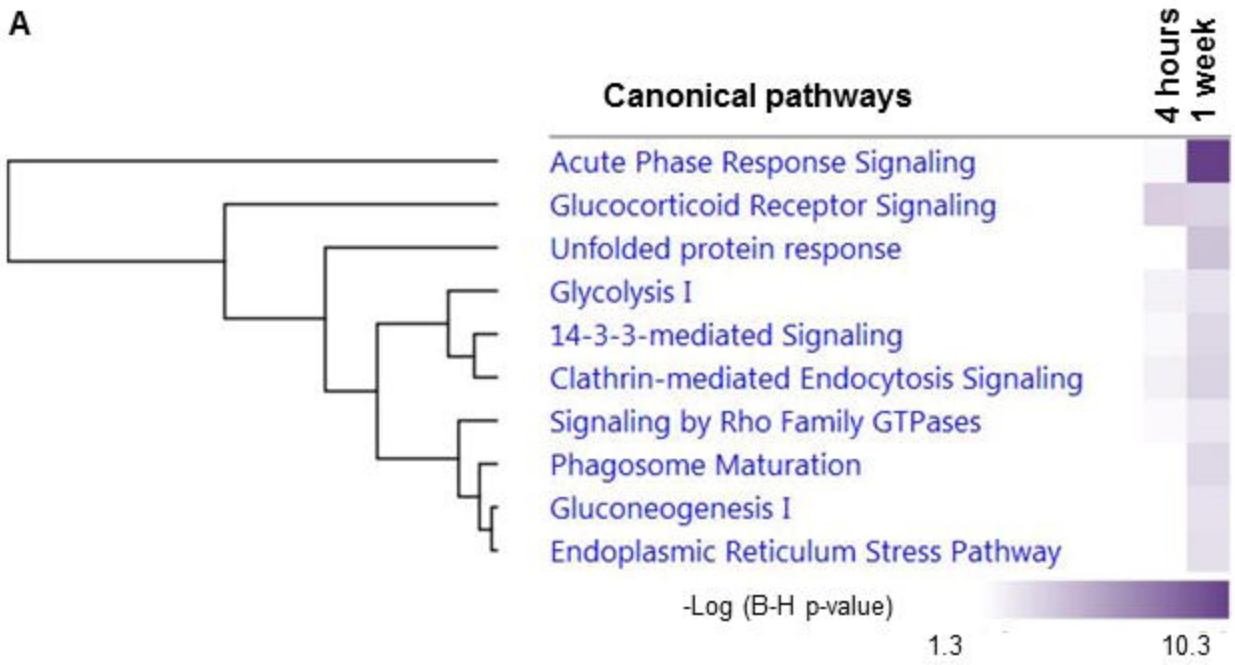
A
Canonical pathways
4 hours
1 week
Acute Phase Response Signaling
Glucocorticoid Receptor Signaling
Unfolded protein response
Glycolysis I
14-3-3-mediated Signaling
Clathrin-mediated Endocytosis Signaling
Signaling by Rho Family GTPases
Phagosome Maturation
Gluconeogenesis I
Endoplasmic Reticulum Stress Pathway
-Log (B-H p-value)
1.3
10.3

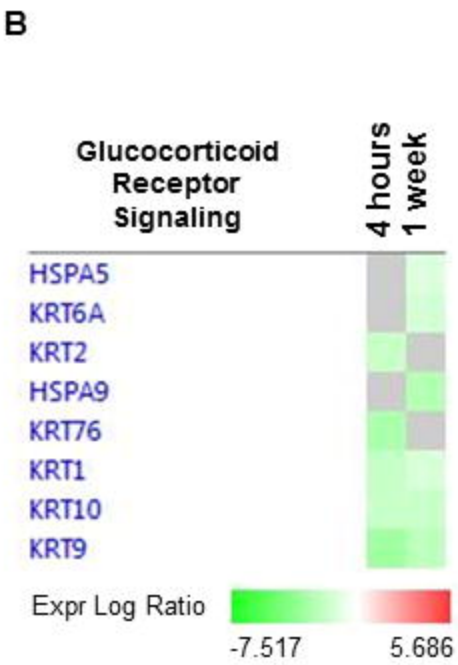
B
Glucocorticoid Receptor Signaling
4 hours
1 week
HSPA5
KRT6A
KRT2
HSPA9
KRT76
KRT1
KRT10
KRT9
Expr Log Ratio
-7.517
5.686

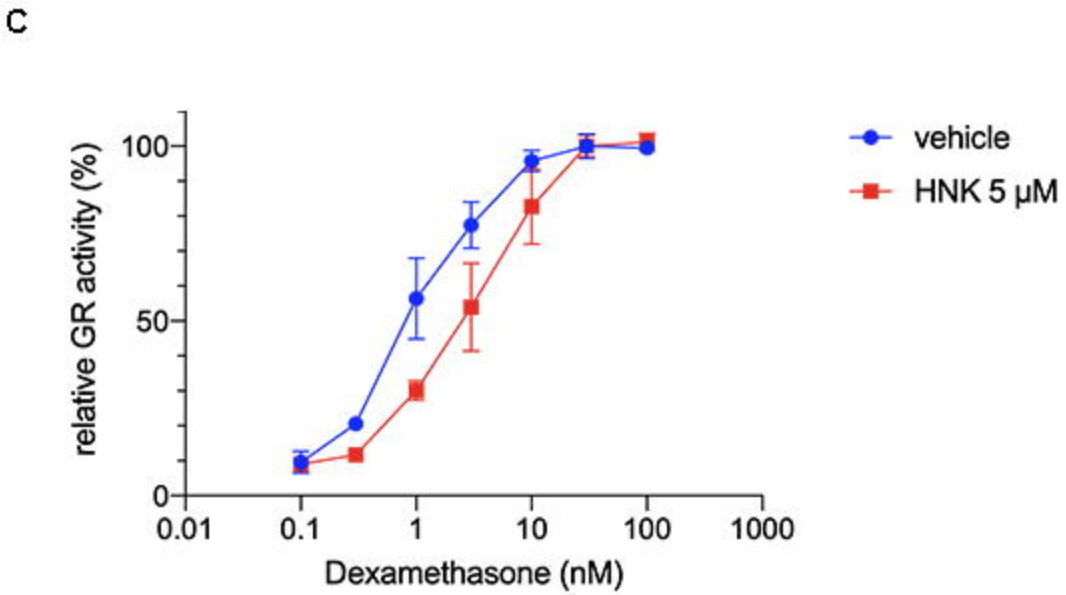
C
relative GR activity (%)
100
50
0
0.01
0.1
1
10
100
1000
Dexamethasone (nM)
vehicle
HNK 5 µM

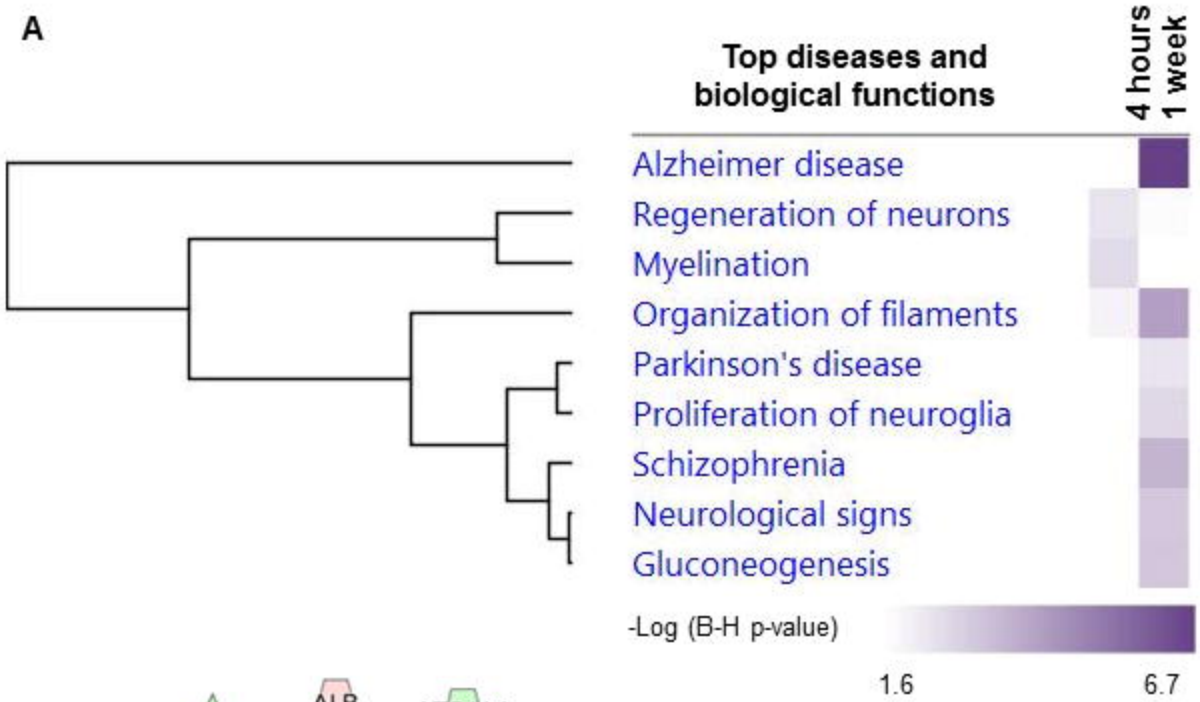
A
Top diseases and biological functions
4 hours
1 week
Alzheimer disease
Regeneration of neurons
Myelination
Organization of filaments
Parkinson's disease
Proliferation of neuroglia
Schizophrenia
Neurological signs
Gluconeogenesis
-Log (B-H p-value)
1.6
6.7

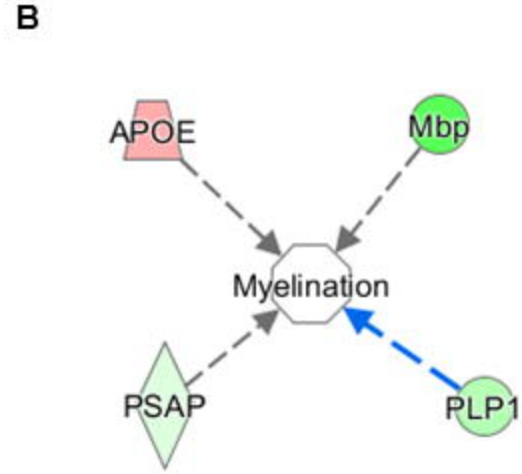
B
APOE
Mbp
Myelination
PSAP
PLP1

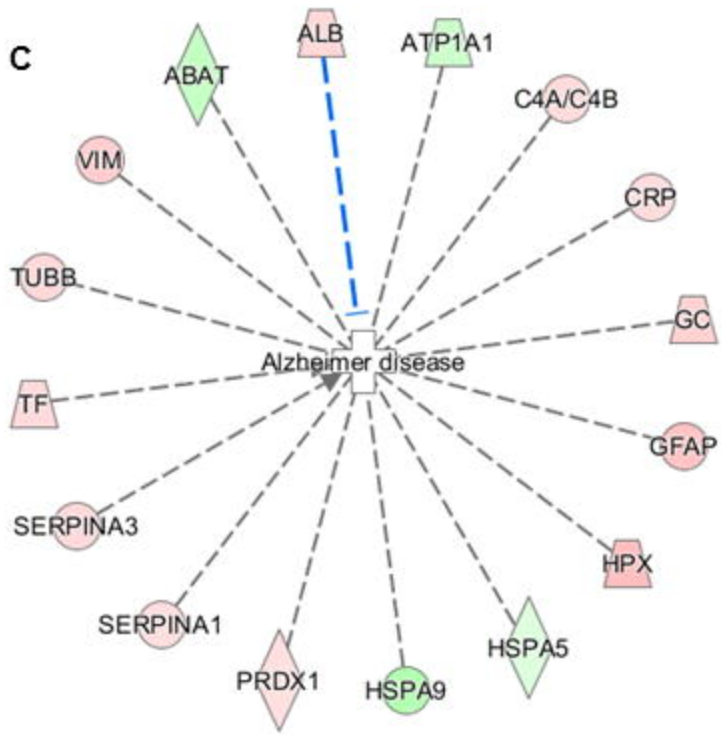
C
ABAT
ALB
ATP1A1
C4A/C4B
VIM
CRP
TUBB
GC
Alzheimer disease
TF
GFAP
SERPINA3
HPX
SERPINA1
HSPA5
PRDX1
HSPA9

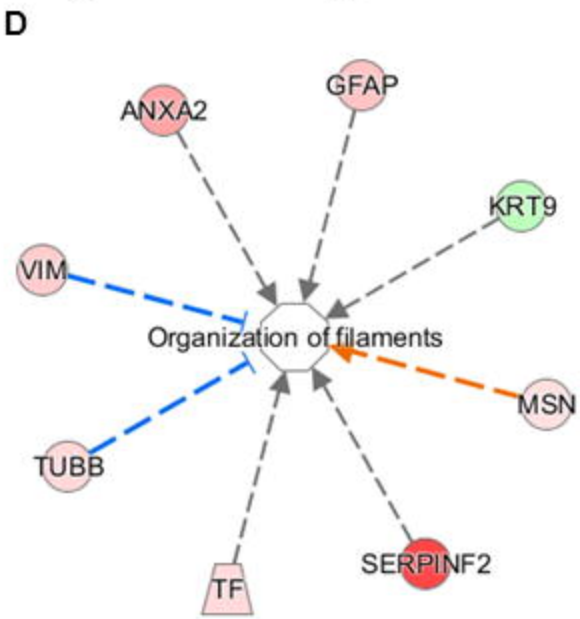
D
ANXA2
GFAP
KRT9
VIM
Organization of filaments
MSN
TUBB
SERPINF2
TF

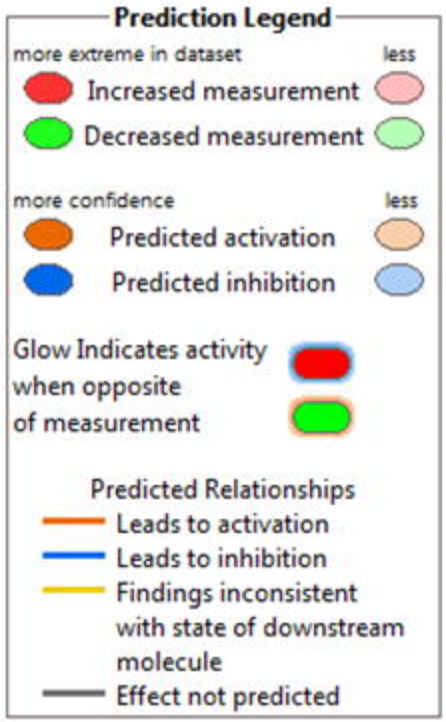
Prediction Legend
more extreme in dataset
less
Increased measurement
Decreased measurement
more confidence
less
Predicted activation
Predicted inhibition
Glow Indicates activity when opposite of measurement
Predicted Relationships
Leads to activation
Leads to inhibition
Findings inconsistent with state of downstream molecule
Effect not predicted

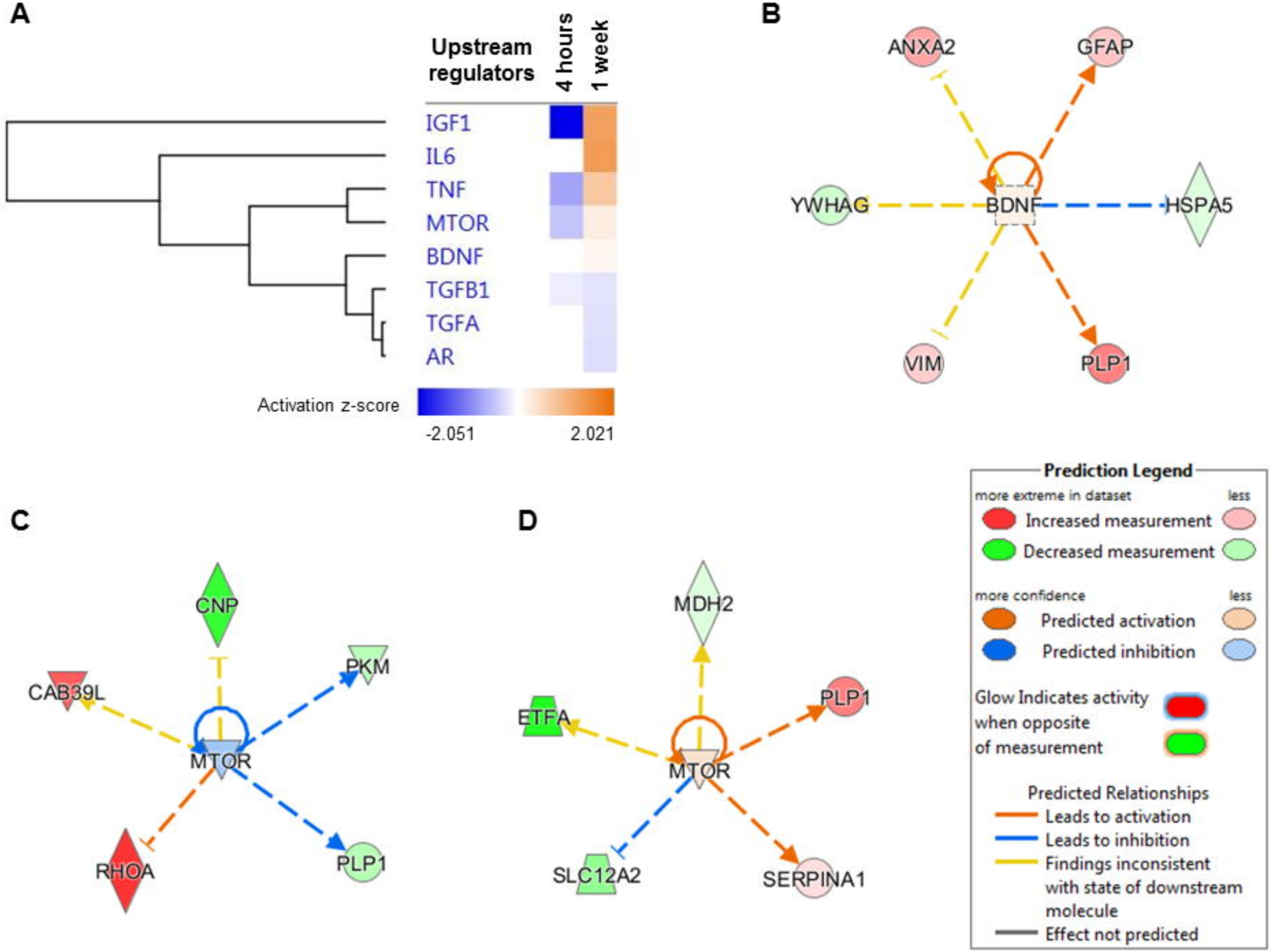
A
Upstream regulators
4 hours
1 week
IGF1
IL6
TNF
MTOR
BDNF
TGFB1
TGFA
AR
Activation z-score
-2.051
2.021
B
ANXA2
GFAP
YWHAG
BDNF
HSPA5
VIM
PLP1
C
CNP
PKM
CAB39L
MTOR
RHOA
PLP1
D
MDH2
PLP1
ETFA
MTOR
SLC12A2
SERPINA1
Prediction Legend
more extreme in dataset
less
Increased measurement
Decreased measurement
more confidence
less
Predicted activation
Predicted inhibition
Glow Indicates activity when opposite of measurement
Predicted Relationships
Leads to activation
Leads to inhibition
Findings inconsistent with state of downstream molecule
Effect not predicted